Analysis of the CDF Biorthogonal MRTD Method With Application to PEC Targets

Xianyang Zhu, *Senior Member, IEEE*, Traian Dogaru, *Member, IEEE*, and Lawrence Carin, *Fellow, IEEE*

***Abstract*—We consider the biorthogonal Cohen–Daubechies–Feauveau (CDF) wavelet family in the context of a biorthogonal multiresolution time-domain (bi-MRTD) analysis. A disadvantage of previous bi-MRTD analyses is an inability to handle abrupt changes in material properties, particularly for a perfect electric conductor (PEC). A multiregion method is proposed to address PEC targets. The proposed method is based on the fact that the CDF bi-MRTD may be viewed as a linear combination of several conventional finite-difference time-domain (FDTD) solutions. The implementation of the connecting surface is also simplified. Several numerical results are presented, with comparison to analytic and FDTD results.**

***Index Terms*—Numerical methods, time domain, wavelets.**

I. Introduction

THE finite-difference time-domain (FDTD) method has been widely used in the field of computational electromagnetics due to its simple implementation and a capability to address complex targets [1]–[3]. From the viewpoint of the moment method, the conventional FDTD is based on a rectangular-pulse field expansion [4]. Poor FDTD numerical dispersion properties are inevitable due to the discontinuous basis functions. As a result, field components have to be oversampled to obtain numerical results with reasonable accuracy. This requirement becomes computationally expensive for electrically large targets.

The multiresolution time-domain (MRTD) method has been proposed recently to improve numerical-dispersion properties [4]–[10]. In the MRTD, wavelet-based basis functions are used spatially, rather than rectangular pulses. Numerical results have shown that much better numerical-dispersion properties are obtained by employing continuous wavelet functions, such as the orthonormal Battle–Lamarie wavelet family [4], [5]. However, this wavelet family is of infinite support spatially and, therefore, basis-function truncation is required in a numerical implementation [4].

To circumvent this, one may use basis functions that are smooth while simultaneously being of compact (finite) support. The Daubechies wavelet family is smooth, orthonormal, and has compact support [11], [12]. An analogous biorthogonal wavelet family developed by Cohen–Daubechies–Feauveau (CDF) [13] has the same properties of smoothness and compact support, while also being symmetric. Biorthogonal multiresolution time domain (bi-MRTD) denotes the MRTD based on the biorthogonal CDF wavelet family [14]–[16]. Numerical examples in [16] demonstrate excellent numerical accuracy with a relatively simple implementation (comparable to the MRTD with other wavelet families [4]).

Most previous MRTD scattering results have been for dielectric targets [4]–[10], [14]–[16]. There are significant complications for the case of targets composed of a perfect electric conductor (PEC). In particular, the principal advantage of the MRTD with smooth basis functions is found in the reduced spatial-sampling requirements. This results in both CPU and memory savings [4], [5], [14]–[16]. However, this reduced spatial-sampling rate also implies that the basis functions are of extended support spatially, complicating enforcement of localized PEC boundary conditions. In this paper, we develop a new formalism by which the bi-MRTD algorithm may be extended to the case of PEC targets. We demonstrate results for isolated PEC targets, as well as PEC-dielectric composite targets.

The remainder of this paper is organized as follows. The bi-MRTD is reviewed briefly in Section II, and a numerical example is presented to show its difficulty in handling PEC targets. In Section III, we propose a new multiregion bi-MRTD implementation to address PEC targets. Numerical results are given in Section IV to show the validity and accuracy of the method, followed by conclusions in Section V.

II. Brief Review of the bi-MRTD

In the view of the moment method [17], the conventional FDTD is based on a rectangular-pulse field expansion in space and time [4]. Similarly, any electric- or magnetic-field component for a three-dimensional problem may be expanded in terms of the duals of the scaling and wavelet functions in the x-, y-, and z-directions constituting the bi-MRTD scheme [14], [15]. Here, we perform a biorthogonal wavelet expansion in space, while retaining the pulse expansion in time.

Without loss of generality, we consider the bi-MRTD implementation with scaling functions alone since the greatest computational savings were found by using such a scheme [15], although it is a single-resolution approach. By adding a level of wavelets (not shown here to simplify the presentation), we obtain the full multiresolution formalism [14], [15]. Under these assumptions, two typical field update equations, in Cartesian coordinates, may be written as

$$E_{x_{i,j,k}}^{m+1} = \alpha E_{x_{i,j,k}}^{m} + \beta \sum_{n=1}^{n_a} a(n) \times \left(H_{z_{i,j+n-1,k}}^{(m+(1/2))} - H_{z_{i,j-n,k}}^{(m+(1/2))} - H_{y_{i,j,k+n-1}}^{(m+(1/2))} + H_{y_{i,j,k-n}}^{(m+(1/2))} \right) \quad (1a)$$

Manuscript received November 23, 2002.

X. Zhu and L. Carin are with the Department of Electrical and Computer Engineering, Duke University, Durham, NC 27708-0291 USA.

T. Dogaru is with the Army Research Laboratory, Adelphi, MD 20783 USA.

Digital Object Identifier 10.1109/TMTT.2003.815874

$$H_{x_{i,j,k}}^{(m+(1/2))} = H_{x_{i,j,k}}^{(m-(1/2))} + \gamma \sum_{n=1}^{n_a} a(n) \times \left(E_{y_{i,j,k+n}}^{m} - E_{y_{i,j,k-n+1}}^{m} - E_{z_{i,j+n,k}}^{m} + E_{z_{i,j-n+1,k}}^{m} \right) \quad (1b)$$

where the indexes i, j, and k denote the discrete-space indexes, and m denotes the time index. The parameter n_a is the stencil size, which is equal to half the number of the nonzero coefficients $a(n)$. These are determined by the scaling function and its dual as follows:

$$a(n) = \int \frac{\partial \widetilde{\phi}_{(n+(1/2))}(x)}{\partial x} \phi_n(x) dx. \quad (2)$$

The other coefficients are defined as in a conventional FDTD analysis, and given as

$$\alpha = \frac{1 - \frac{\sigma \Delta t}{2\varepsilon}}{1 + \frac{\sigma \Delta t}{2\varepsilon}} \quad (3a)$$

$$\beta = \frac{\Delta t}{\varepsilon \Delta x \left(1 + \frac{\sigma \Delta t}{2\varepsilon} \right)} \quad (3b)$$

$$\gamma = \frac{\Delta t}{\mu \Delta x} \quad (3c)$$

where parameters ε, μ, and σ represent the permittivity, permeability, and conductivity of the material, respectively. Parameters Δx and Δt denote the spatial grid size and time-step size. Coefficients $a(n)$ for different stencil sizes and various biorthogonal bases may be found in [11].

Field coefficient updating (1) are valid for a homogeneous medium. Theoretically, one may handle the material heterogeneity in a rigorous way by introducing "heterogeneity matrices" in the update equations [6], [7]. However, this would significantly complicate the implementation of the algorithm, especially if the stencil size is large. In the case of the CDF scaling functions, the nondiagonal elements of these matrices are very small and can be neglected, thus, the material electrical properties can be sampled point-wise, similar to the FDTD algorithm. The CDF family also meets many of the requirements of an efficient MRTD scheme: maximum number of wavelet-function vanishing moments for a given support, good regularity for the dual wavelet functions, and symmetry.

Previous results in [14] have shown that bi-MRTD demonstrates better numerical dispersion properties relative to the conventional FDTD method. For the examples in [16], the spatial sampling rate may be reduced by a factor of two while obtaining the same level of accuracy, resulting in substantial savings in both RAM and CPU time. The computational savings afforded by bi-MRTD are function of the target's electrical size since this dictates the numerical-dispersion properties; the savings vis-à-vis FDTD increase as the target size increases.

However, for PEC targets, a more accurate description of the target boundaries is required. A simple locally homogeneous representation is no longer enough to attain good numerical results. A typical numerical result is shown in Fig. 1, where the far-field scattered signal from a PEC sphere is compared in

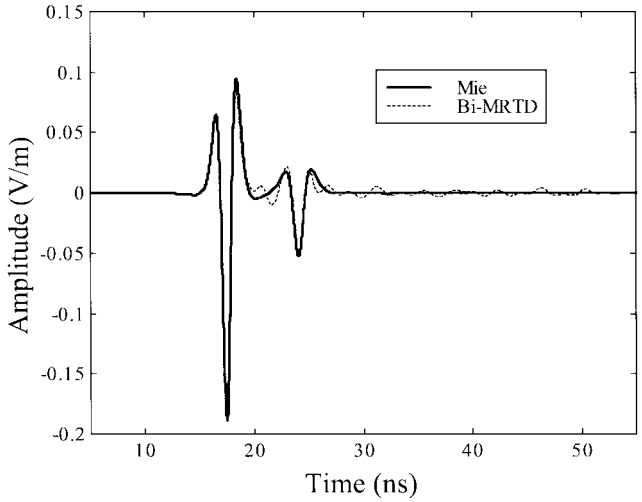

(a)

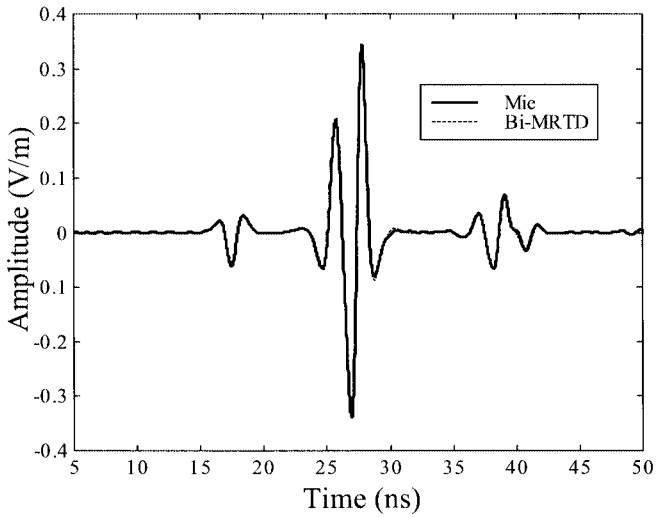

(b)

Fig. 1. Far-zone fields of a PEC and dielectric sphere by using bi-MRTD directly without any modification. The radius of the sphere is 0.375 m for both cases, and the incident wave is a fourth-order Rayleigh pulse with central frequency of 400 MHz. (a) PEC sphere (spatial sampling rate is approximately 20 points per wavelength at the highest frequency). (b) Dielectric sphere with relative permittivity of 4.0 (spatial sampling rate is approximately ten points per wavelength at the highest frequency).

Fig. 1(a) with the Mie-series solution. The radius of the sphere is 0.375 m, and the incident wave is a transient fourth-order Rayleigh pulse [18] with central frequency at 400 MHz. The spatial sampling rate is approximately 20 points per wavelength at the highest frequency. The agreement between the two results is good for the first response; this signal due to specular reflection off the front face of the target. However, we also see that the difference between the two results is large for the second transient response, and many spurious ripples exist at late times. In these results, we set to zero those scaling-function coefficients associated with electric-field components that are tangential to the target interface. For comparison, we also present the computed far field of a same-sized dielectric sphere in Fig. 1(b). All the geometrical parameters are the same as for the PEC case, although the spatial sampling rate is actually approximately ten points per wavelength inside the medium

at the highest frequency since the relative permittivity of the medium employed here is $\varepsilon_r = 4$. Excellent agreement is observed between the numerical and analytic solutions, as in previous bi-MRTD implementations for dielectric targets [14]–[16]. The challenge addressed in this paper involves extending the bi-MRTD to PEC targets, with the goal of achieving comparable accuracy as achieved for dielectric targets.

III. New View of the bi-MRTD Method and a Multiregion Scheme

A. Multiregion bi-MRTD Formalism

Without loss of generality, and as an example, we rewrite (1a) as

$$\begin{aligned} E_{x_{i,j,k}}^{m+1} =& \alpha E_{x_{i,j,k}}^{m} + a(1)\beta_1 \left(H_{z_{i,j,k}}^{(m+(1/2))} - H_{z_{i,j-1,k}}^{(m+(1/2))} \right. \\ & \left. - H_{y_{i,j,k}}^{(m+(1/2))} + H_{y_{i,j,k-1}}^{(m+(1/2))} \right) \\ & + 3a(2)\beta_2 \left(H_{z_{i,j+1,k}}^{(m+(1/2))} - H_{z_{i,j-2,k}}^{(m+(1/2))} \right. \\ & \left. - H_{y_{i,j,k+1}}^{(m+(1/2))} + H_{y_{i,j,k-2}}^{(m+(1/2))} \right) \\ & + \ldots + (2n_a - 1)a(n_a)\beta_{n_a} \\ & \times \left(H_{z_{i,j+n_a-1,k}}^{(m+(1/2))} - H_{z_{i,j-n_a,k}}^{(m+(1/2))} - H_{y_{i,j,k+n_a-1}}^{(m+(1/2))} \right. \\ & \left. + H_{y_{i,j,k-n_a}}^{(m+(1/2))} \right) \end{aligned} \tag{4}$$

where coefficients β_1, β_2, and β_{n_a} are defined as follows:

$$\beta_1 = \beta \tag{5a}$$

$$\beta_2 = \frac{\Delta t}{\varepsilon 3\Delta x \left(1 + \dfrac{\sigma \Delta t}{2\varepsilon}\right)} \tag{5b}$$

$$\beta_{n_a} = \frac{\Delta t}{\varepsilon (2n_a - 1)\Delta x \left(1 + \dfrac{\sigma \Delta t}{2\varepsilon}\right)}. \tag{5c}$$

The coefficients a must satisfy the following requirement for the numerical result to converge to the exact solution as the spatial grid size approaches zero [14]:

$$\sum_{n=1}^{n_a} a(n)(2n-1) = 1. \tag{6}$$

Thus, (4) may be broken into n_a different sub-equations

$$\begin{aligned} a(1)E_{x_{i,j,k}}^{m+1} =& a(1)\alpha E_{x_{i,j,k}}^{m} + a(1)\beta_1 \\ & \times \left(H_{z_{i,j,k}}^{(m+(1/2))} - H_{z_{i,j-1,k}}^{(m+(1/2))} \right. \\ & \left. - H_{y_{i,j,k}}^{(m+(1/2))} + H_{y_{i,j,k-1}}^{(m+(1/2))} \right) \end{aligned} \tag{7a}$$

$$\begin{aligned} 3a(2)E_{x_{i,j,k}}^{m+1} =& 3a(2)\alpha E_{x_{i,j,k}}^{m} + 3a(2)\beta_2 \\ & \times \left(H_{z_{i,j+1,k}}^{(m+(1/2))} - H_{z_{i,j-2,k}}^{(m+(1/2))} \right. \\ & \left. - H_{y_{i,j,k+1}}^{(m+(1/2))} + H_{y_{i,j,k-2}}^{(m+(1/2))} \right) \end{aligned} \tag{7b}$$

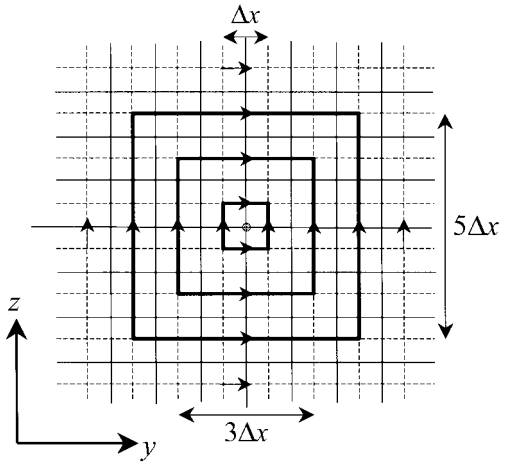

Fig. 2. CDF $(2,2)$ bi-MRTD algorithm viewed as a linear combination of three conventional FDTD methods.

$$\begin{aligned} & \ldots \\ (2n_a - 1)a(n_a)E_{x_{i,j,k}}^{m+1} =& (2n_a - 1)a(n_a)\alpha E_{x_{i,j,k}}^{m} \\ & + (2n_a - 1)a(n_a)\beta_{n_a} \\ & \times \left(H_{z_{i,j+n_a-1,k}}^{(m+(1/2))} - H_{z_{i,j-n_a,k}}^{(m+(1/2))} \right. \\ & \left. - H_{y_{i,j,k+n_a-1}}^{(m+(1/2))} + H_{y_{i,j,k-n_a}}^{(m+(1/2))} \right). \end{aligned} \tag{7c}$$

One may observe that the bi-MRTD algorithm is actually a linear combination of n_a conventional FDTD ones with spatial grid sizes equal to Δx, $3\Delta x, \ldots$, and $(2n_a - 1)\Delta x$. Fig. 2 shows that the CDF $(2,2)$ bi-MRTD (stencil size of three) may be viewed as a linear combination of three conventional FDTD algorithms. Three blackened rectangles in Fig. 2 represent three integral contours corresponding to three different conventional FDTD schemes with grid sizes of Δx, $3\Delta x$, and $5\Delta x$. It is important to note that an analogous decomposition may be effected for MRTD with orthonormal Daubechies wavelets [11] and for Battle–Lemarie wavelets [4], [5]. Therefore, this development should be of general interest to the MRTD community.

The three coefficients $a(1)$, $a(2)$, and $a(3)$ for the CDF $(2,2)$ basis are 1.2291667, -0.0937500, and 0.0104167. Therefore, the contribution of all 12 magnetic fields around the electric field is weighted by one of these coefficients according to its distance to the electric-field point. The closer the distance is, the more contribution it will generate.

This relationship between the bi-MRTD and conventional FDTD is important for algorithm implementation. We demonstrate next how it may be used to address bi-MRTD analysis of PEC targets.

B. Multiregion Scheme for the PEC Targets

The FDTD analysis of scattering from arbitrary shaped PEC targets has proven to be a challenge. Many conformal techniques have been developed in the last several years. Many of them use curvilinear coordinates or nonorthogonal grids [19]–[23] in order to perfectly describe the target boundaries.

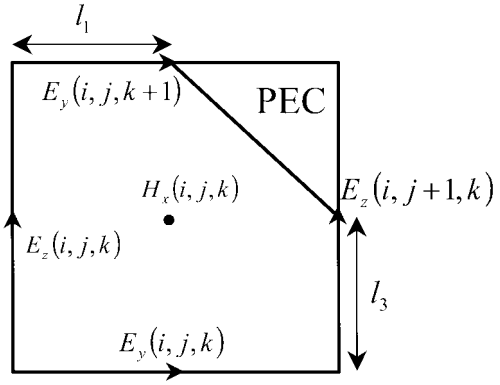

Fig. 3. Schematic drawing of a partially filled FDTD cell.

However, curvilinear coordinates cannot be easily extended for arbitrary shaped structures, and the nonorthogonal FDTD usually requires much longer CPU time due to the complexity of the algorithm. This vitiates the simplicity and efficiency of the conventional FDTD, two of its most important characteristics. Therefore, more recent algorithms are based on a locally conformal technique [24]–[32]. A major advantage of this approach is that only local cells around the boundaries of the targets need be specially treated. Both dielectric and PEC targets may be handled in similar ways.

Generally, the locally conformal techniques are based on the integral form of the Maxwell's equations. We will employ the scheme proposed in [28]. Consider a cell partially filled by a PEC, as shown in Fig. 3, the magnetic field H_x inside the cell is updated slightly differently compared with the conventional FDTD algorithm. The corresponding update equation reads

$$H_{x_{i,j,k}}^{(m+(1/2))} = H_{x_{i,j,k}}^{(m-(1/2))} + \frac{\Delta t}{\mu \Delta s}\left[\left(l_1 E_{y_{i,j,k+1}}^{m} - l_2 E_{y_{i,j,k}}^{m}\right) - \left(l_3 E_{z_{i,j+1,k}}^{m} - l_4 E_{z_{i,j,k}}^{m}\right)\right] \tag{8}$$

where Δs is the area of the whole cell, l_1, l_2, l_3, and l_4 are the lengths of the non-PEC part of the four edges. Update equations for the other magnetic fields may be deduced in a similar manner. If $l_i < \Delta x/2 (i = 1, 2, 3,$ or $4)$, then the electric field on the corresponding edge should be borrowed from the neighboring edges. An efficient linear interpolation [31] may be employed for simplicity.

As discussed before, the bi-MRTD method cannot be applied to the PEC directly by simply setting to zero the samples of the electric-field components tangential to the boundary. To deal with this problem, we define subregions around the PEC targets. The aforementioned locally conformal FDTD may be applied inside the subregions, using the FDTD-like representation in (7). The key innovation here is that the FDTD-based decomposition in (7) allows us to exploit previous developments in FDTD analysis of PEC targets. The conventional bi-MRTD algorithm is used in the rest of the computational domain. It is noted that the fields are consistent in or outside the sub-domains and, hence, there are no numerical instabilities.

C. Implementation of the Connecting Surface

In general, the MRTD basis-function coefficients do not represent the field components at the corresponding position of the MRTD grid. To obtain the field component at a specific point, we must weigh the basis-function coefficients by the appropriate basis functions. That is, the field at a given point is determined by several neighboring basis-function coefficients. Consequently, the implementation of the MRTD connecting surface should be more complicated than that for the conventional FDTD method [15] (because the extended MRTD basis functions yield less spatial localization vis-à-vis the FDTD). To make the update equations consistent through the boundary of the connecting surface, appropriate incident field components should be compensated for in the region around the connecting surface with support dictated by the stencil size [15]. This requires much RAM to store the corresponding incident field components, especially for a large stencil size.

However, the interpolating property of the CDF scaling functions [33] simplifies this procedure. In particular, we can prove that, if the fields are represented in the scaling-function space alone (no further wavelet levels are considered in the expansion), then the field sample at one given grid point equals the scaling coefficient corresponding to that point. To demonstrate this, consider the following representation of the continuous E_x component (only spatial dimensions are considered here):

$$E_x(x,y,z) = \sum_{i,j,k=-\infty}^{\infty} E_{x,i,j,k}^{\Phi} \widetilde{\Phi}_i(x) \widetilde{\Phi}_j(y) \widetilde{\Phi}_k(z). \tag{9}$$

To obtain the value of this field component at the point of coordinates (x_0, y_0, z_0) corresponding to grid point (i_0, j_0, k_0), we sample the expression above with a three-dimensional delta pulse centered at that point as follows:

$$\begin{aligned} E_x(x_0,y_0,z_0) &= \int\int\int E_x(x,y,z)\delta(x-x_0)\delta(y-y_0) \\ &\quad \times \delta(z-z_0)dxdydz \\ &= \int\int\int \sum_{i,j,k=-\infty}^{\infty} E_{x,i,j,k}^{\Phi} \widetilde{\Phi}_i(x)\widetilde{\Phi}_j(y)\widetilde{\Phi}_k(z) \\ &\quad \times \delta(x-i_0\Delta x)\delta(y-j_0\Delta x) \\ &\quad \times \delta(z-k_0\Delta x)dxdydz \\ &= \sum_{i,j,k} E_{x,i,j,k}^{\Phi} \widetilde{\Phi}_i(i_0\Delta x)\widetilde{\Phi}_j(j_0\Delta x) \\ &\quad \times \widetilde{\Phi}_k(k_0\Delta x). \end{aligned} \tag{10}$$

Now we make use of the interpolating property of the CDF dual scaling functions, which states that (m and m' being any integers)

$$\widetilde{\Phi}_m(m'\Delta x) = \delta_{m-m'}. \tag{11}$$

It is easy to see that we obtain the result mentioned above, i.e., $E_x(x_0,y_0,z_0) = E_{x,i_0,j_0,k_0}^{\Phi}$. The practical implication on the bi-MRTD implementation is that we can always make a direct conversion from field samples to scaling expansion coefficients and vice-versa. Regarding the incident field implementation, only one layer of scaling coefficients around the connecting surface is required for compensation of the incident fields [1]. The RAM used to store the incident waves can be reduced to $1/n_a$

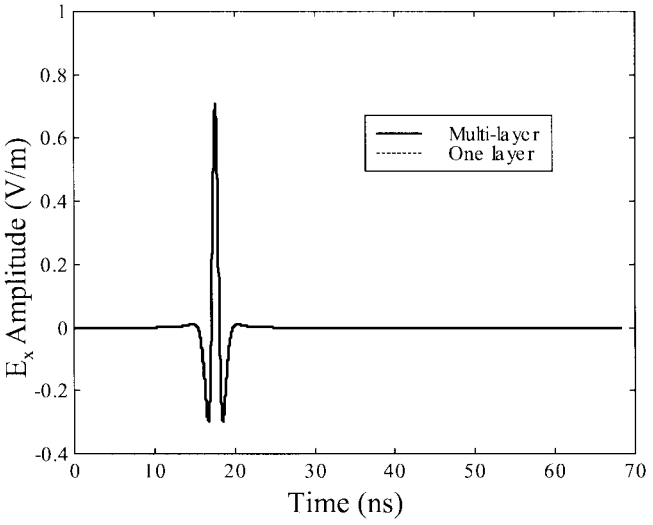

(a)

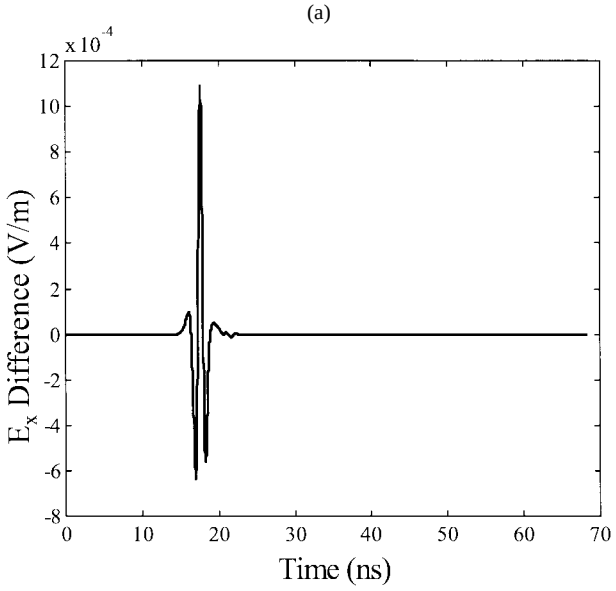

(b)

Fig. 4. Comparison of the two different implementations of the connecting surface. No target is placed inside the computational domain. The incident wave and sampling rate are the same as those in Fig. 1. The incident angles are $\phi_i = 0$ and $\theta_i = 45^\circ$. (a) Comparison of the E_x-field component, computed using a single and multilayer connecting surface. (b) Difference between the results in (a).

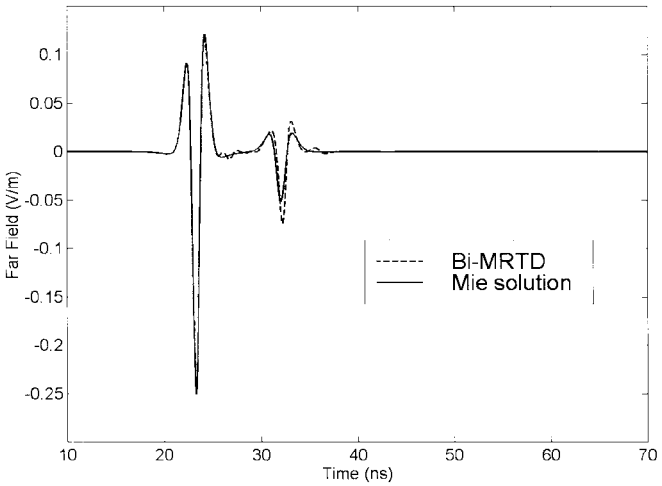

(a)

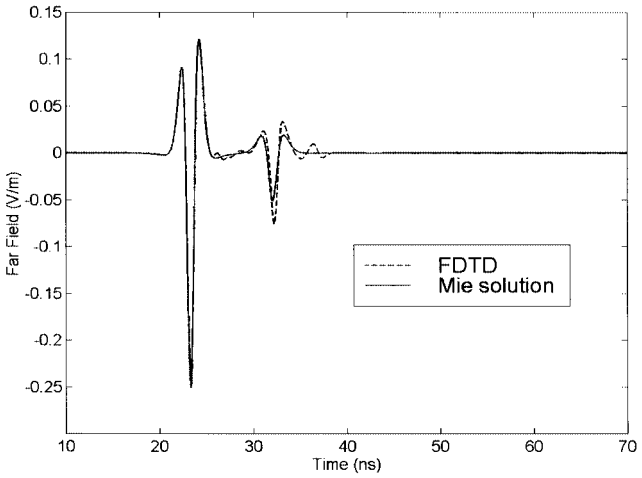

(b)

Fig. 5. Computed far field of a PEC sphere by using the multiregion bi-MRTD scheme and the FDTD. The radius of the PEC sphere is 0.5 m, and the incident wave is a fourth-order Rayleigh pulse with central frequency of 400 MHz. The spatial sampling rate is approximately 15 points per wavelength at the highest frequency. (a) Bi-MRTD result compared with the Mie solution. (b) FDTD result compared with the Mie solution.

of that of a general MRTD scheme. It is also interesting to notice that a similar argument can be employed when storing the equivalent currents on the Huygens surface for the far-zone field calculation: only one layer of scaling coefficients needs to be taken into the calculation on each side of the surface since they represent the field samples at those locations.

The validity of the new implementation is shown in Fig. 4, where the field at a point inside the connecting surface is presented. The incident wave is a fourth-order Rayleigh pulse, and no scatterer is placed inside the computational domain. The pulse shape should be the same as that of the incident wave. The parameters of the incident wave and sampling rate are the same as those in Fig. 1. The incident angles are $\phi_i = 0$ and $\theta_i = 45^\circ$. From Fig. 4, we observe that the fields obtained by the two schemes (old connecting-surface implementation [15], [16] and that presented above) agree with each other very well.

IV. Numerical Results

A. Far Field of a PEC Sphere

We first consider a PEC sphere in free space. The choose a PEC-sphere target because: 1) the sphere is a three-dimensional smooth target that allows examination of the conformal MRTD discussed in Section III-C and 2) the results may be compared to a reference Mie-series solution.

For this numerical example, the sphere radius is 0.5 m, and the incident field is a transient plane wave with the amplitude governed by a fourth-order Rayleigh pulse. The central frequency of the pulse is 400 MHz. The spatial sampling rate is approximately 15 points per wavelength at the highest frequency. As indicated in Section III-C, the locally conformal FDTD method is applied to a subregion in which the PEC sphere resides, and the conventional bi-MRTD algorithm is utilized in the rest of the computational domain.

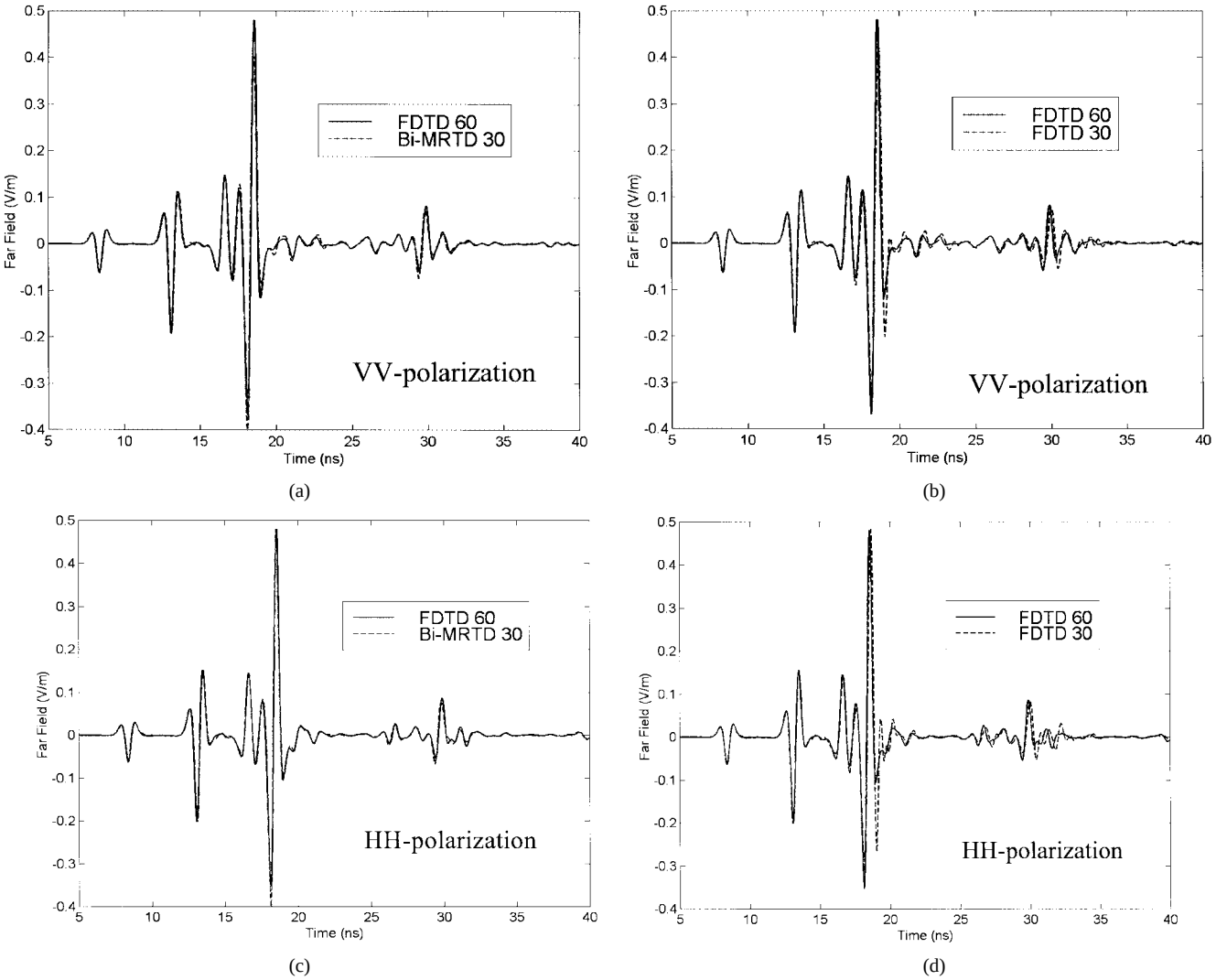

Fig. 6. Far-field scattered field from two spheres (one is a PEC, and the other is a dielectric) by using the multiregion bi-MRTD scheme. The radius of the two spheres is 0.375 m, and the distance between the two centers is 1.125 m. The relative permittivity of the dielectric is 4.0. The incident wave is a fourth-order Rayleigh pulse with a central frequency of 800 MHz, and the incident angles are $\phi_i = 0$ and $\theta_i = 45°$. For bi-MRTD, the spatial sampling rate is 30 points per wavelength (ppw) at the central frequency (5 ppw at the highest frequency). For FDTD, 30 and 60 ppw are used at the central frequency. The FDTD solution with 60 ppw is used as the reference. (a) VV polarization, bi-MRTD 30. (b) VV polarization, FDTD 30. (c) HH polarization, bi-MRTD 30. (d) HH polarization, FDTD 30.

The far field of the PEC sphere is shown in Fig. 5. The three curves represent: 1) the results of an analytical Mie-series solution; 2) conventional FDTD with a staircase approximation to the sphere surface; and 3) the multiregion bi-MRTD method. We observe that the bi-MRTD-generated ripples in the late-time response in Fig. 1 are now absent, and the numerical results of the multiregion bi-MRTD algorithm agree with the analytical solution well. Small differences exist for the staircase FDTD solution, with these removed if an analogous conformal FDTD solution is applied.

In this example, the perfectly matched layer (PML) [1], [2] absorber is placed just a few cells away from the PEC sphere, and the creeping wave attenuates to zero quickly after the initial specular reflection. The advantages of the bi-MRTD solution are more evident for problems in which the time-domain signal is of more-extended support, such problems offering greater opportunities for numerical dispersion. In the following examples, we consider multiple targets, for which inter-target interactions yield a more-complicated scattered signal (longer temporal support).

B. Far Field of Two Spheres

We consider two spheres, one a PEC and the other a dielectric with $\varepsilon_r = 4$. The radius of both the PEC and dielectric spheres is 0.375 m. The center of each sphere is placed along the x-axis, and the distance between the two sphere centers is 1.125 m. The incident angles are $\phi_i = 0$ and $\theta_i = 45°$. Backscattered far fields for both VV and HH polarization are shown in Fig. 6. The central frequency of the fourth-order Rayleigh pulse [18] is 800 MHz. For the multiregion bi-MRTD scheme, the spatial sampling rate is approximately five points per wavelength inside the dielectric sphere at the highest frequency.

Three curves are presented in Fig. 6. Besides the result of the multiregion bi-MRTD scheme, the other two curves are the numerical results of two conventional FDTD schemes with sampling rates of five and ten points per wavelength inside the di-

electric sphere at the highest frequency. There is no analytical result for this example case, thus, the finely sample conventional-FDTD results provide a reference (running the FDTD results with a higher sampling rate yielded results comparable to the ten-points-per-wavelength data mentioned above).

From Fig. 6, we observe that the agreement between the multiregion bi-MRTD scheme and the finer grid FDTD method is generally good, while the numerical dispersion is evident in the FDTD results with the same sampling rate as that of the multiregion bi-MRTD.

C. Tilted Infinitesimally Thin PEC Plate

As a final example, we consider the bistatic radar cross section (RCS) for scattering from an infinitesimally thin PEC sheet. Computations are performed in the time domain, and results are shown (after Fourier transform) for the case in which the electrical length of the square sheet is one wavelength on a side (this corresponds to an actual frequency, in the computations, of 1.6 GHz). Reference results are computed via the FDTD sampled at 40 cells per wavelength. In these reference computations, the PEC sheet lies in the (x, y) plane of a Cartesian coordinate system such that there is no need in this case for a conformal formulation. The angle of incidence is $\theta_i = 45^\circ$ and $\phi_i = 0^\circ$. To examine the accuracy of the conformal formulation, we now tilt the PEC sheet at a 45° angle in the same Cartesian coordinate system, and adjust the angle of incidence accordingly. Ideally, the results from the reference FDTD computation should be identical to those generated for the tilted PEC sheet.

For the tilted-sheet results, we consider a spatial sample rate of 20 cells per wavelength at the frequency of interest, and two sets of results are considered. In one, we use a traditional FDTD formulation with a staircase (stepwise) approximation to the surface of the PEC sheet; in the second set of results, we employ the conformal MRTD solution developed here. The bi-static RCS is presented in Fig. 7. As indicated in Fig. 7, the conformal results are generally considerably closer to the reference solution than the staircase FDTD solution. When the staircase approximation is applied at a sample rate of 40 cells per wavelength, the level agreement is comparable to that of the conformal MRTD solution. These results underscore the principal utility of a conformal solution: it allows one to sample space at a coarser spatial sampling rate, reducing computational costs, while still yielding accurate results.

D. Numerical Stability

When one modifies the original FDTD or MRTD framework to incorporate a conformal mesh, the original stability conditions in these algorithms may be undermined. It has been demonstrated by Craddock *et al.* [34] that the conformal approach considered here, originally developed in [28], has the potential of becoming unstable. In [34], methodologies are presented to mitigate this problem. It is our experience, based on the results presented here, and on numerous other examples, that the algorithm has displayed no problems with numerical instability. This is not to say it can *never* become unstable, but we have not observed any such problems in our studies based on an extensive set of numerical experiments. However, this is a topic worthy of further study, with an even wider range of problems, and potentially the conformal formulation presented here may be modified as in [34].

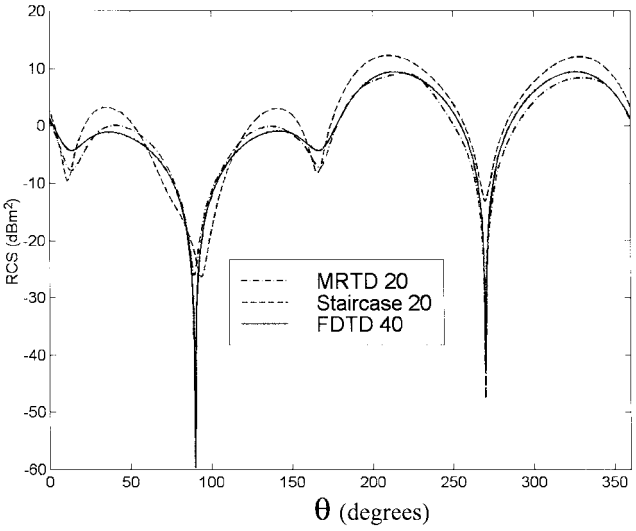

Fig. 7. Bistatic RCS from a tilted PEC sheet. The reference FDTD results sampled at 40 cells per wavelength correspond to the plate positioned in the (x, y) plane, and the results for sampling at 20 cells per wavelength correspond to the plate tilted 45°. The results for the tilted plate are presented here with the angle of observation converted to the corresponding angle for the flat plate, allowing a direct comparison. The electric field is polarized in the θ direction.

V. Conclusions

Although the bi-MRTD algorithm yields better numerical dispersion properties relative to the conventional FDTD method, it cannot be directly applied to the case of PEC targets. This is because the field components in bi-MRTD are defined over an extended spatial grid, mitigating implementation of localized PEC boundary conditions. The key development of this paper is that, with a reorganization of the bi-MRTD update equations, this algorithm may be viewed as a linear combination of several conventional FDTD sets of equations. The number of conventional FDTD equation is equal to the stencil size of the bi-MRTD coefficients. The most important interpretation of the linear combination is that the field coefficients obtained through the bi-MRTD update equations do represent the field components at corresponding points in space. On the basis of this observation, a multiregion bi-MRTD scheme has been proposed to deal with scattering from PEC targets, i.e., the conventional conformal FDTD algorithm is used inside all the subregions where the PEC targets reside, and the bi-MRTD algorithm is employed in the rest of the computational domain. Numerical examples show that the multiregion bi-MRTD scheme is a successful tool for dealing with PEC targets.

The implementation of the connecting surface and the calculation of the equivalent currents on the Huygens' surface may also be simplified. In particular, the associated field components need only be stored on a single layer (as opposed to over the multiple layers of the MRTD stencil), yielding significant RAM savings.

REFERENCES

[1] A. Taflove and S. C. Hagness, *Computational Electromagnetics: The Finite-Difference Time-Domain Method*. Norwood, MA: Artech House, 2000.

[2] K. S. Kunz and R. J. Luebbers, *The Finite Difference Time Domain Method for Electromagnetics*. Boca Raton, FL: CRC Press, 1993.

[3] A. Taflove, Ed., *Advances in Computational Electrodynamics: The Finite-Difference Time-Domain Method*. Norwood, MA: Artech House, 1998.

[4] M. Krumpholz and L. P. B. Katehi, "MRTD: New time domain schemes based on multiresolution analysis," *IEEE Trans. Microwave Theory Tech.*, vol. 44, pp. 555–572, Apr. 1996.

[5] E. M. Tentzeris, A. Cangellaris, L. P. B. Katehi, and J. Harvey, "Multiresolution time-domain (MRTD) adaptive schemes using arbitrary resolution wavelets," *IEEE Trans. Microwave Theory Tech.*, vol. 50, pp. 501–516, Feb. 2002.

[6] T. Dogaru and L. Carin, "Application of Haar-wavelet-based multiresolution time-domain schemes to electromagnetic scattering problems," *IEEE Trans. Antennas Propagat.*, vol. 50, pp. 774–784, June 2002.

[7] X. Zhu and L. Carin, "Multiresolution time-domain analysis of plane wave scattering from general three-dimensional surface and subsurface dielectric targets," *IEEE Trans. Antennas Propagat.*, vol. 49, pp. 1568–1578, Nov. 2001.

[8] M. Fujii and W. J. R. Hoefer, "A three-dimensional Haar-wavelet-based multiresolution analysis similar to the FDTD method-derivation and application," *IEEE Trans. Microwave Theory Tech.*, vol. 46, pp. 2463–2475, Dec. 1998.

[9] E. M. Tentzeris, R. L. Robertson, J. Harvey, and L. P. B. Katehi, "Stability and dispersion analysis of Battle–Lemarie based MRTD schemes," *IEEE Trans. Microwave Theory Tech.*, vol. 47, pp. 1004–1013, July 1999.

[10] T. Dogaru and L. Carin, "Multiresolution time-domain analysis of scattering from a rough dielectric surface," *Radio Sci.*, vol. 35, pp. 1279–1292, Nov.–Dec. 2000.

[11] I. Daubechies, *Ten Lectures on Wavelets*. Philadelphia, PA: SIAM, 1992.

[12] M. Fujii and W. J. R. Hoefer, "Dispersion of time domain wavelet Galerkin method based on Daubechies' compactly supported scaling functions with three and four vanishing moments," *IEEE Microwave Guided Wave Lett.*, vol. 10, pp. 125–127, Apr. 2000.

[13] A. Cohen, I. Daubechies, and J. C. Feauveau, "Biorthogonal bases of compactly supported wavelets," *Pure Appl. Math.*, vol. 45, pp. 485–560, 1992.

[14] T. Dogaru and L. Carin, "Multiresolution time-domain using CDF biorthogonal wavelets," *IEEE Trans. Microwave Theory Tech.*, vol. 49, pp. 902–912, May 2001.

[15] X. Zhu, T. Dogaru, and L. Carin, "Three-dimensional biorthogonal multiresolution time-domain method and its application to electromagnetic scattering problems," *IEEE Trans. Antennas Propagat.*, to be published.

[16] ——, "Parallel implementation of the biorthogonal MRTD method," *J. Opt. Soc. Amer. A, Opt. Image Sci.*, vol. 20, pp. 844–855, May 2003.

[17] R. F. Harrington, *Field Computation by Moment Methods*. Piscataway, NJ: IEEE Press, 1993.

[18] P. Hubral and M. Tygel, "Analysis of the Rayleigh pulse," *Geophysics*, vol. 54, pp. 654–658, 1989.

[19] P. H. Harms, J. Lee, and R. Mittra, "A study of the nonorthogonal FDTD method versus the conventional FDTD technique for computing resonant frequencies of cylindrical cavities," *IEEE Trans. Microwave Theory Tech.*, vol. 40, pp. 741–746, Apr. 1992.

[20] M. Fusco, "FDTD algorithm in curvilinear coordinates," *IEEE Trans. Antennas Propagat.*, vol. 38, pp. 76–89, Jan. 1990.

[21] B. J. McCartin and J. F. DiCello, "Three-dimensional finite difference frequency domain scattering using the control region approximation," *IEEE Trans. Magn.*, vol. 25, pp. 3092–3094, July 1989.

[22] R. Holland, "Finite difference solutions of Maxwell's equations in generalized nonorthogonal coordinates," *IEEE Trans. Nucl. Sci.*, vol. NS-30, pp. 4589–4591, Dec. 1983.

[23] J. F. Lee, R. R. Palandech, and R. Mittra, "Modeling three-dimensional discontinuities in waveguides using nonorthogonal FDTD algorithm," *IEEE Trans. Microwave Theory Tech.*, vol. 40, pp. 346–352, Feb. 1992.

[24] N. Kaneda, B. Houshmand, and T. Itoh, "FDTD analysis of dielectric resonators with curved surfaces," *IEEE Trans. Microwave Theory Tech.*, vol. 45, pp. 1645–1649, Sept. 1997.

[25] S. Dey, R. Mittra, and S. Chebolu, "A technique for implementing the FDTD algorithm on a nonorthogonal grid," *Microwave Opt. Technol. Lett.*, vol. 14, no. 4, pp. 213–215, Mar. 1997.

[26] S. Dey and R. Mittra, "A locally conformal finite-difference time-domain (FDTD) algorithm for modeling three-dimensional perfectly conducting objects," *IEEE Microwave Guided Wave Lett.*, vol. 7, pp. 273–275, Sept. 1997.

[27] ——, "A modified locally conformal finite-difference time-domain algorithm for modeling three-dimensional perfectly conducting objects," *Microwave Opt. Technol. Lett.*, vol. 17, no. 6, pp. 349–352, Apr. 1998.

[28] W. Yu and R. Mittra, "A conformal FDTD algorithm for modeling perfectly conducting objects with curve-shaped surfaces and edges," *Microwave Opt. Technol. Lett.*, vol. 27, no. 2, pp. 136–138, Oct. 2000.

[29] S. Dey and R. Mittra, "A conformal finite-difference time-domain technique for modeling cylindrical dielectric resonators," *IEEE Trans. Microwave Theory Tech.*, vol. 47, pp. 1737–1739, Sept. 1999.

[30] W. Yu and R. Mittra, "A conformal finite difference time domain technique for modeling curved dielectric surfaces," *IEEE Microwave Wireless Comp. Lett.*, vol. 11, pp. 25–27, Jan. 2001.

[31] Y. Zhang, L. Li, and C. Liang, "A modified locally conformal FDTD for broadwall radiating slot in a finite wall thickness waveguide," *Microwave Opt. Technol. Lett.*, vol. 35, no. 3, pp. 198–201, Nov. 2002.

[32] X. Zhong and K. K. Mei, "An improved conformal FDTD algorithm of modeling planar microwave structures," *Microwave Opt. Technol. Lett.*, vol. 35, no. 3, pp. 219–224, Nov. 2002.

[33] W. Sweldens and R. Piessens, "Wavelet sampling techniques," in *Proceedings of the Statistical Computing Section*. Alexandria, VA: Amer. Stat. Assoc., 1993, pp. 20–29.

[34] I. J. Craddock, C. J. Railton, and J. P. McGeehan, "Derivation and application of a passive equivalent circuit for the finite difference time domain algorithm," *IEEE Microwave Guided Wave Lett.*, vol. 6, pp. 40–42, Jan. 1996.

Xianyang Zhu (M'00–SM'02) was born in Anhui, China, in 1967. He received the B.S. and Ph.D. degrees in electrical engineering from the Xi'an Jiaotong University, Xi'an, China, in 1988 and 1994, respectively.

From 1994 to 1997, he was with the Electromagnetics Institute, Southwest Jiaotong University, Sichuan, China, where, in 1995, he became an Associate Professor. From November 1997 to February 1999, he was a Post-Doctoral Research Fellow with the Center for Computational Electromagnetics, Department of Electrical and Computer Engineering, University of Illinois at Urbana-Champaign. Since March 1999, he has been a Research Associate with the Center for Applied Remote Sensing, Department of Electrical and Computer Engineering, Duke University, Durham, NC. His current research interests include computational electromagnetics, radar cross-sectional analysis, rough surface scattering, parallel computation, antenna analysis, and multiresolution time-domain method.

Traian Dogaru (S'96–M'99) was born in Bucharest, Romania, in 1966. He received the engineering degree from the Polytechnic University of Bucharest, Bucharest, Romania, in 1990, and the M.S. degree in electrical engineering and Ph.D. degree from Duke University, Durham, NC, in 1997 and 1999, respectively.

From 1992 to 1995, he has held different engineering positions in the magnetic recording industry. From 1999 to 2001, he was a Research Associate with Duke University, where he developed algorithms for electromagnetic-field modeling. He is currently with the Army Research Laboratory, Adelphi, MD, where his main interests are electromagnetic wave theory, computational electromagnetics, rough surface scattering, and radar-related signal processing.

Lawrence Carin (SM'96–F'01) was born on March 25, 1963, in Washington, DC. He received the B.S., M.S., and Ph.D. degrees in electrical engineering from the University of Maryland at College Park, in 1985, 1986, and 1989, respectively.

In 1989, he joined the Electrical Engineering Department, Polytechnic University, Brooklyn, NY, as an Assistant Professor, and became an Associate Professor in 1994. In September 1995, he joined the Electrical Engineering Department, Duke University, Durham, NC, where he is currently a Professor. He was the Principal Investigator (PI) on a Multidisciplinary University Research Initiative (MURI) on demining (1996–2001). He is currently the PI of a MURI dedicated to multimodal inversion. His current research interests include short-pulse scattering, subsurface sensing, and wave-based signal processing.

Dr. Carin is a member of Tau Beta Pi and Eta Kappa Nu. He is an associate editor of the IEEE TRANSACTIONS ON ANTENNAS AND PROPAGATION.